Supplementary Information

Differential activation mechanisms of lipid GPCRs by lysophosphatidic acid and sphingosine 1-phosphate

Shian Liu, Navid Paknejad, Lan Zhu, Yasuyuki Kihara, Manisha Ray, Jerold Chun, Wei Liu, Richard K. Hite, and Xin-Yun Huang

Supplementary Table 1. Cryo-EM data collection, refinement and validation statistics of $S1P_1$ structures.

	S1P– $S1P_1$–$G\alpha_{i1}\beta_1\gamma_2$	Siponimod–$S1P_1$–$G\alpha_{i1}\beta_1\gamma_2$
Data collection and processing		
Magnification	81000	81000
Voltage (kV)	300	300
Electron exposure ($e^-/Å^2$)	24.65	23.44
Defocus range (μm)	-0.8 to -1.5	-0.8 to -1.5
Pixel size (Å)	1.083	1.083
Symmetry imposed	C1	C1
Initial particle images (no.)	4,460,634	11,076,739
Final particle images (no.)	449,331	1,789,970
Map resolution (Å)	3.0	2.6
FSC threshold	0.143	0.143
Map sharpening *B* factor ($Å^2$)	122.6	116.7
Refinement		
Initial model used (PDB code)	3V2Y 1GP2	3V2Y 1GP2
Model resolution (Å)	3.08	2.81
FSC threshold	0.5	0.5
Model composition		
Non-hydrogen atoms	7035	6902
Protein residues	909	894
Ligands	2	2
B factors ($Å^2$)		
Protein	44.66	42.35
Ligand	55.70	58.17
R.m.s. deviations		
Bond lengths ($Å^2$)	0.004	0.005
Bond angles (°)	0.46	0.47
Validation		
MolProbity score	1.57	1.57
Clashscore	2.43	3.3
Poor rotamers (%)	0	0
Ramachandran plot		
Favored (%)	95.31	95.11
Allowed (%)	4.69	4.89
Disallowed (%)	0	0

Supplementary Table 2. Cryo-EM data collection, refinement and validation statistics of LPA_1 structures.

	LPA–LPA_1–$G\alpha_{i1}\beta_1\gamma_2$	LPA–LPA_1–$G\alpha_{i1}\beta_1\gamma_2$ (State a)	LPA–LPA_1–$G\alpha_{i1}\beta_1\gamma_2$ (State a')
Data collection and processing			
Magnification	22,500	22,500	22,500
Voltage (kV)	300	300	300
Electron exposure ($e^-/Å^2$)	28.2	28.2	28.2
Defocus range (μm)	-0.8 to -2.2	-0.8 to -2.2	-0.8 to -2.2
Pixel size (Å)	1.064	1.064	1.064
Symmetry imposed	C1	C1	C1
Initial particle images (no.)	2,235,123	1,579,604	1,579,604
Final particle images (no.)	1,588,791	31,567	32,504
Map resolution (Å)	2.83	3.08	3.11
FSC threshold	0.143	0.143	0.143
Map sharpening *B* factor ($Å^2$)	-145.7	-74.9	-77.8
Refinement			
Initial model used (PDB code)	4Z34 1GP2	4Z34 1GP2	4Z34 1GP2
Model resolution (Å)	2.95	3.23	3.18
FSC threshold	0.5	0.5	0.5
Model composition			
Non-hydrogen atoms	7095	7151	7139
Protein residues	904	907	906
Ligands	1	1	1
B factors ($Å^2$)			
Protein	60.82	67.82	67.36
Ligand	61.02	60.91	65.18
R.m.s. deviations			
Bond lengths ($Å^2$)	0.002	0.002	0.002
Bond angles (°)	0.422	0.400	0.385
Validation			
MolProbity score	1.50	1.08	0.94
Clashscore	2.70	2.74	2.04
Poor rotamers (%)	0	0	0
Ramachandran plot			
Favored (%)	96.63	98.10	98.88
Allowed (%)	3.37	1.90	1.12
Disallowed (%)	0	0	0

$S1P_1$ $G\alpha_i$ $\beta_1\gamma_2$ w/ sphingosine-1-phosphate (S1P)
Cryo-EM Acquisition & Processing

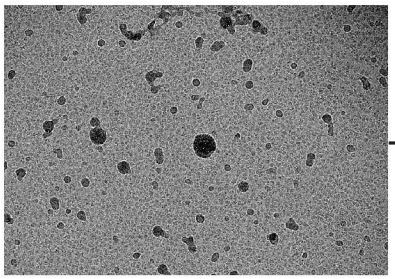

3970 micrographs
Krios w/ Gatan K3
Binned to 1.064 pixel size (super-resolution mode)

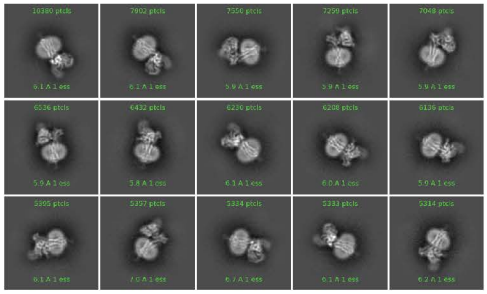

CtfFind4.1.13 CTF Estimation
Relion 3.1b LoG particle picking (over-pick)
Extract

CryoSparc v2.14.2 Heterogeneous Classifications (Iterate)

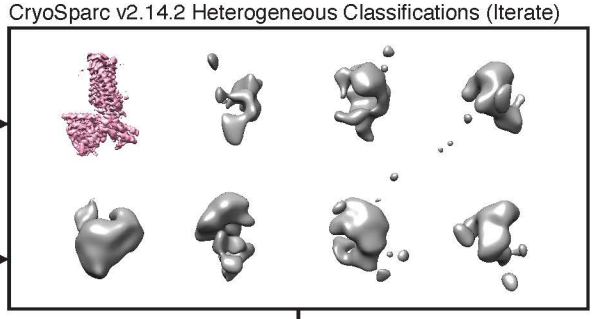

Iterate

CryoSparc v2.14.2 2D Classification (Validate Results)
CryoSparc v2.14.2 Non-Uniform Refinement

1) Relion 3.1b Bayesian Polishing
2) CryoSparc v2.14.2 Local CTF Refinement
3) CryoSparc v2.14.2 Global CTF Refinement
4) Phenix v1.17.1-3660 Density Modification

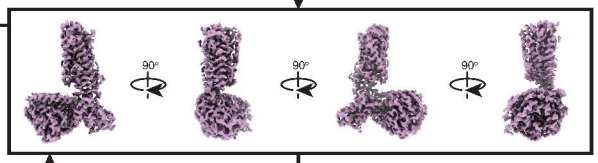

Mask Creation ($S1P_1$ and $G\alpha_i\beta_1\gamma_2$)
CryoSparc v2.14.2 Local Refinement
Phenix v1.17.1-3660 Density Modification

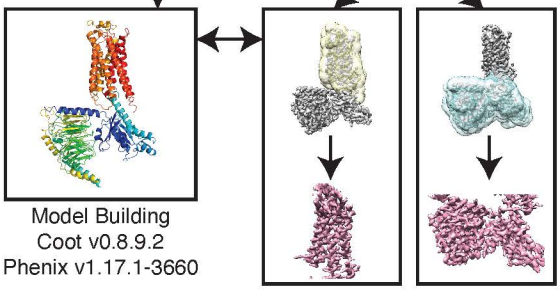

Model Building
Coot v0.8.9.2
Phenix v1.17.1-3660

Half-Map FSC

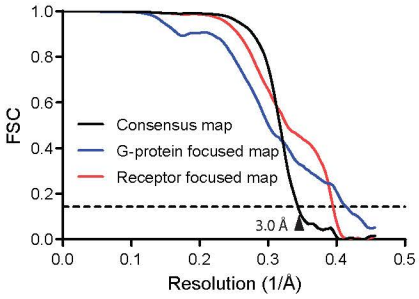

Density-modified Half-Map FSC

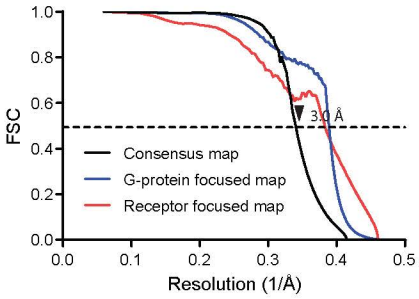

Map-to-Model FSC

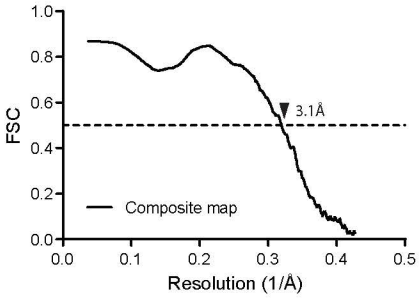

Local Resolution Map

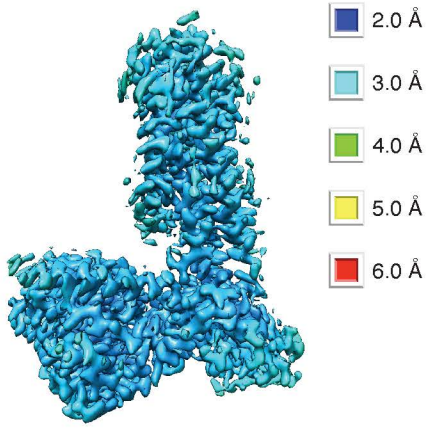

CryoSparc v2.15.0 Local Resolution Estimation
FSC Cut-Off = 0.5

Supplementary Figure 1. Cryo-EM data acquisition and processing. In short, 3970 micrographs were collected with low dose and close to focus on a FEI Krios with Gatan K3 direct electron detector. Heterogeneous refinement was used to remove false positive particles, with 2D classification as a form of verification. Once an ideal particle stack was identified, subsequent rounds of heterogeneous refinement were combined with local CTF refinement, Bayesian polishing, and global CTF refinement to further improve the map. Local refinements of S1P1 and Gi helped bring out features in the periphery of the structure. The model was built into the density-modified consensus and local refinements, with the final round of real-space refinement being run against a composite map of the two local refinements generated in Phenix. Overall, most of the model was well represented by density. The alpha-helical domain was less well resolved due to flexibility, and thus not built into the final model.

S1P$_1$ Gα_i $\beta_1\gamma_2$ w/ siponimod
Cryo-EM Acquisition & Processing

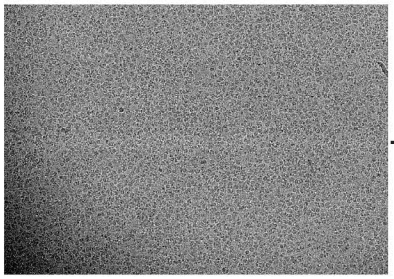

5171micrographs
Krios w/ Gatan K3
Binned to 1.064 pixel size (super-resolution mode)

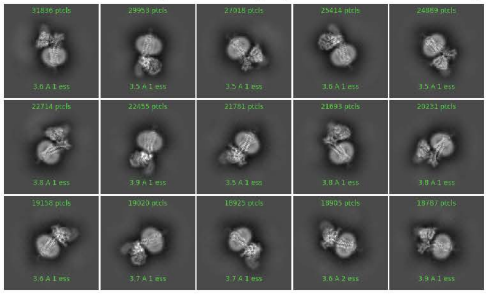

GCTF v1.18 CTF Estimation
Relion 3.1b LoG particle picking (over-pick)
Extract

CryoSparc v2.15.0 Heterogeneous Classifications (Iterate)

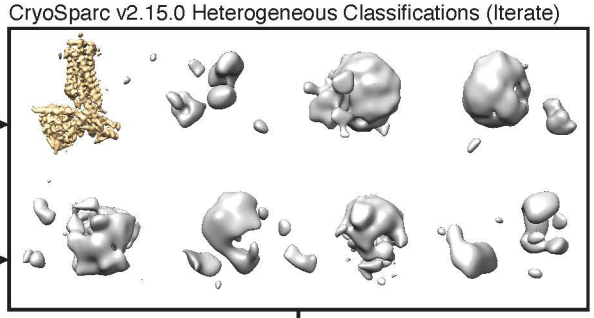

Iterate

CryoSparc v2.15.0 2D Classification (Validate Results)
CryoSparc v2.15.0 Non-Uniform Refinement

1) Relion 3.1b Bayesian Polishing
2) CryoSparc v2.15.0 Local CTF Refinement
3) CryoSparc v2.15.0 Global CTF Refinement
4) Phenix v1.17.1-3660 Density Modification

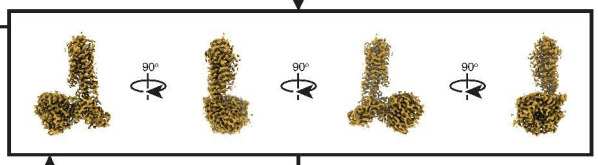

Mask Creation (S1P$_1$ and G$\alpha_i\beta_1\gamma_2$)
CryoSparc v2.15.0 Local Refinement
Phenix v1.17.1-3660 Density Modification

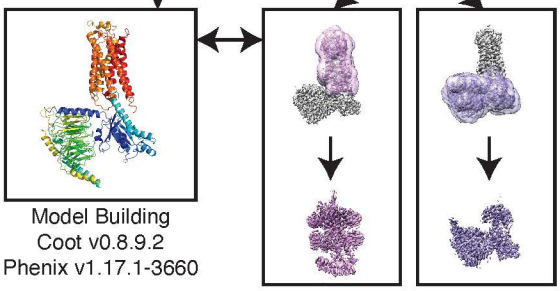

Model Building
Coot v0.8.9.2
Phenix v1.17.1-3660

Half-Map FSC

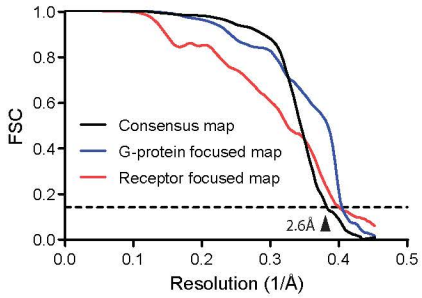

Density-modified Half-Map FSC

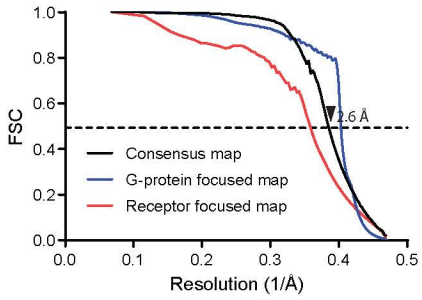

Map-to-Model FSC

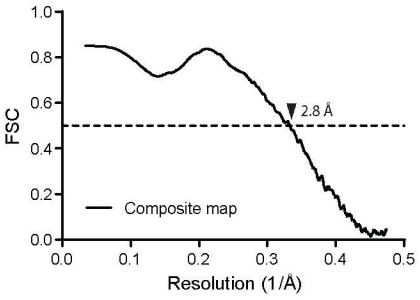

Local Resolution Map

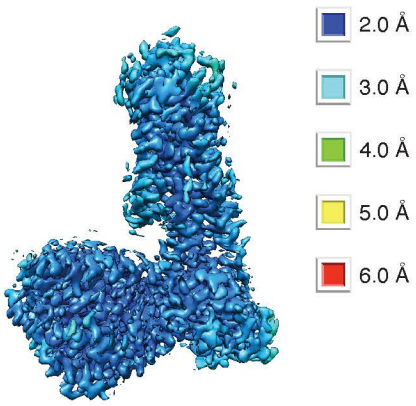

CryoSparc v3.1.0 Local Resolution Estimation
FSC Cut-Off = 0.5

Supplementary Figure 2. Cryo-EM data acquisition and processing. In short, 5171 micrographs were collected with low dose and close to focus on a FEI Krios with Gatan K3 direct electron detector. Heterogeneous refinement was used to remove false positive particles, with 2D classification as a form of verification. Once an ideal particle stack was identified, subsequent rounds of heterogeneous refinement were combined with local CTF refinement, Bayesian polishing, and global CTF refinement to further improve the map. Local refinements of S1P1 and Gi helped bring out features in the periphery of the structure. The model was built into the density-modified consensus and local refinements, with the final round of real-space refinement being run against a composite map of the two local refinements generated in Phenix. Overall, most of the model was well represented by density. The alpha-helical domain was less well resolved due to flexibility, and thus not built into the final model.

LPA$_1$ Gα$_i$ β$_1$γ$_2$ w/ Lysophosphatidic Acid
Cryo-EM Acquisition & Processing

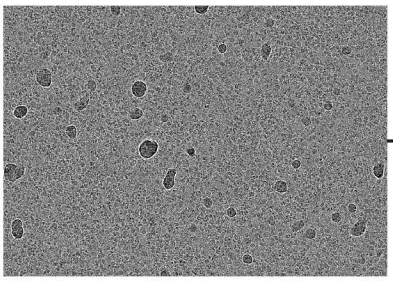

10050 micrographs
Krios w/ Gatan K3
Binned to 1.064 pixel size (super-resolution mode)

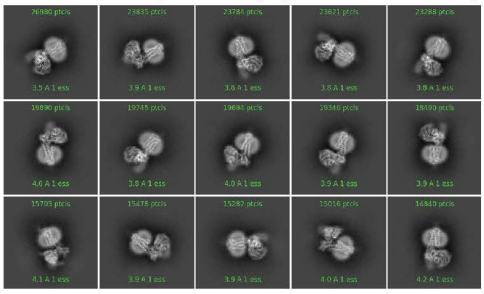

GCTF v1.18 CTF estimation
Relion 3.1b LoG particle picking (over-pick)
Extract

CryoSparc v2.15.0 Heterogeneous Classifications (Iterate)

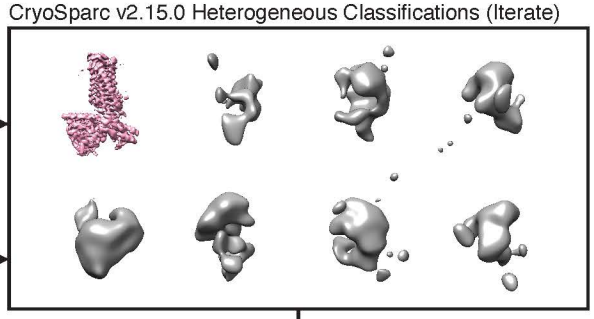

Iterate

CryoSparc v2.15.0 2D Classification (Validate Results)
CryoSparc v2.15.0 Non-Uniform Refinement

1) Relion 3.1b Bayesian Polishing
2) CryoSparc v2.15.0 Local CTF Refinement
3) CryoSparc v2.15.0 Global CTF Refinement
4) Phenix v1.17.1-3660 Density Modification

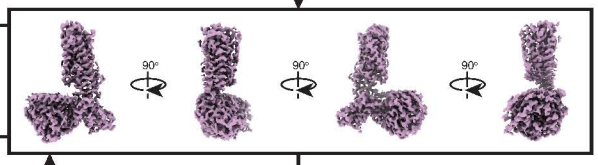

CryoSparc v2.15.0
3D Variability Analysis

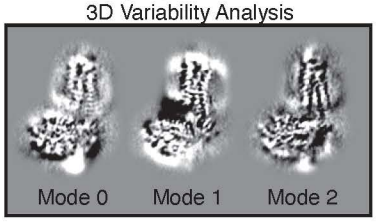

Mask Creation (LPA$_1$ and Gα$_i$β$_1$γ$_2$)
CryoSparc v2.15.0 Local Refinement
Phenix v1.17.1-3660 Density Modification

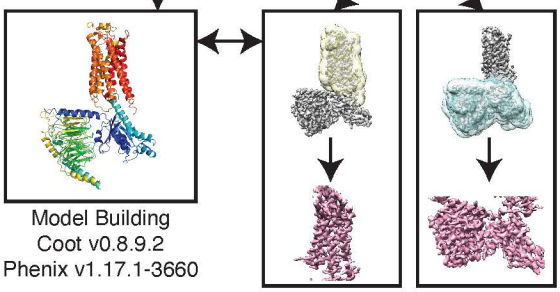

Model Building
Coot v0.8.9.2
Phenix v1.17.1-3660

Half-Map FSC

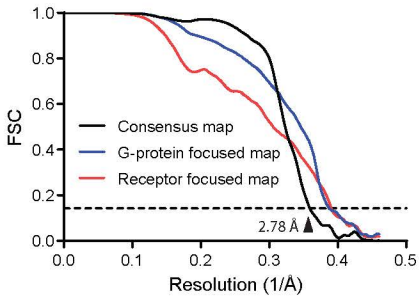

Local Resolution Map

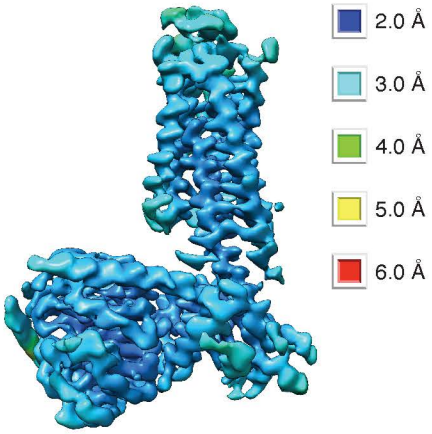

CryoSparc v2.15.0 Local Resolution Estimation
FSC Cut-Off = 0.5

Density-modified Half-Map FSC

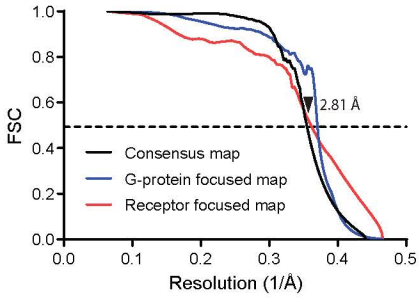

Map-to-Model FSC

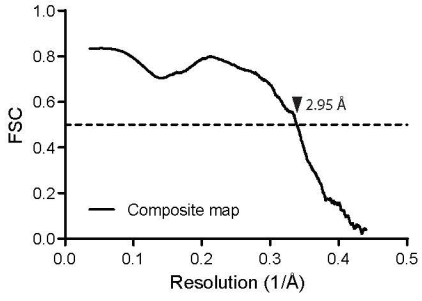

Supplementary Figure 3: Cryo-EM data processing. In short, 10050 micrographs were collected with low dose and close to focus on a FEI Krios with Gatan K3 direct electron detector. Heterogeneous refinement was used to remove false positive particles, with 2D classification as a form of verification. Once an ideal particle stack was identified, subsequent rounds of heterogeneous refinement were combined with local CTF refinement, Bayesian polishing, and global CTF refinement to further improve the map. Local refinements of LPA$_1$ and Gi helped bring out features in the periphery of the structure. The model was built into the density-modified consensus and local refinements, with the final round of real-space refinement being run against a composite map of the two local refinements generated in Phenix. Overall, most of the model was well represented by density. The alpha-helical domain was less well resolved due to flexibility, and thus not built into the final model.

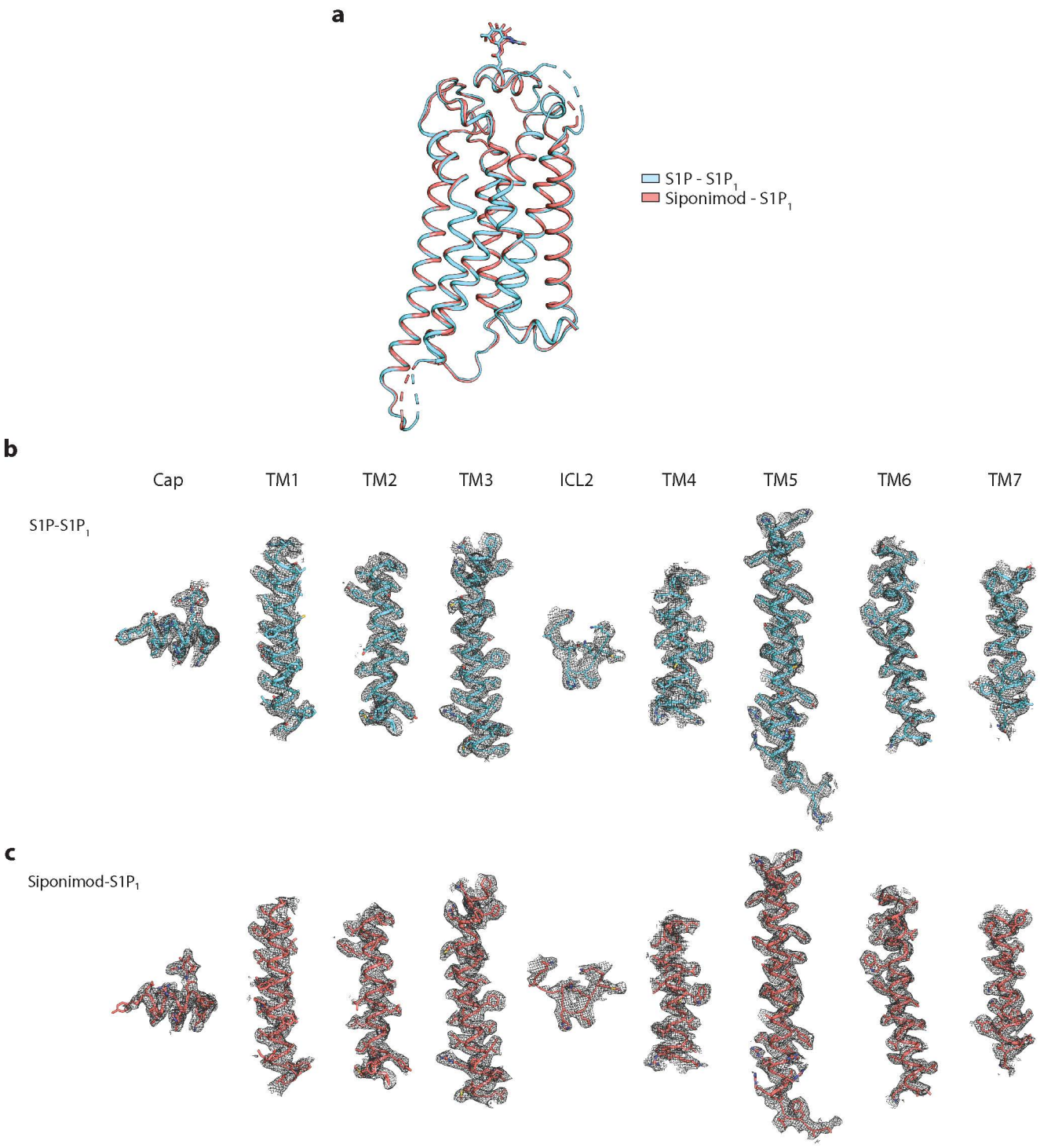

Supplementary Figure 4. **Electron microscopy density maps**. **a**, Comparison of the structures of S1P–$S1P_1$ and siponimod –$S1P_1$. **b,c**, Cryo-EM map quality. Representative densities and fitted models are shown for $S1P_1$ in the S1P–$S1P_1$-Gi complex (**b**), and in the siponimod–$S1P_1$-Gi complex (**c**).

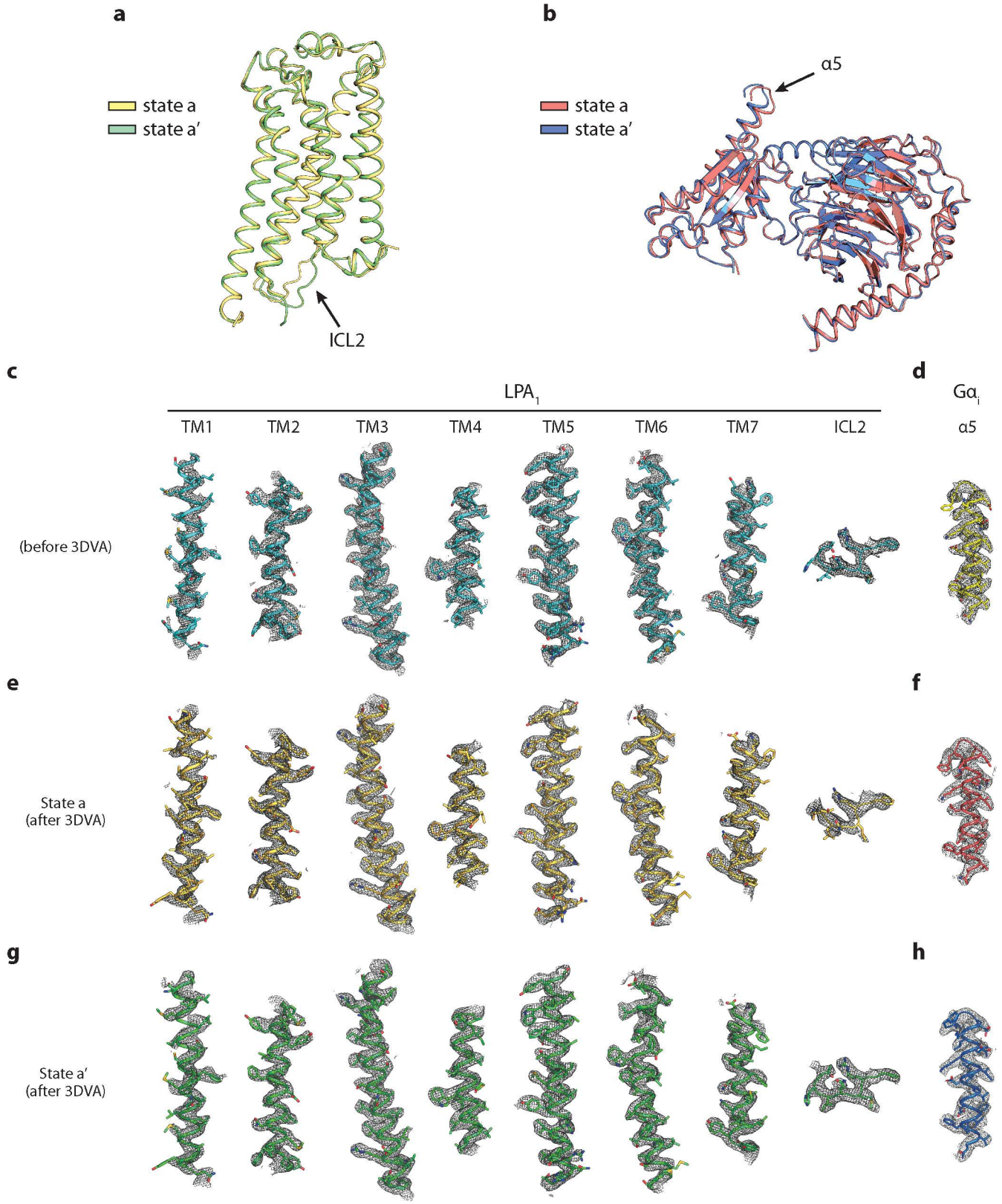

Supplementary Figure 5. **Cryo-EM maps**. **a,b**, Comparison of State a and a' from the first component of 3DVA. Superposition of the two structural models aligned for the receptor (**a**) or Gi (**b**). Black arrows indicate the major conformational changes. **c-h**, Cryo-EM map quality. Representative densities and fitted models are shown for LPA_1 in the state before 3DVA analysis (**c**), State a after 3DVA (**e**), and State a' after 3DVA (**g**), as well as the α5-helices of $G\alpha_i$ (**d, f, h**) in the three states.

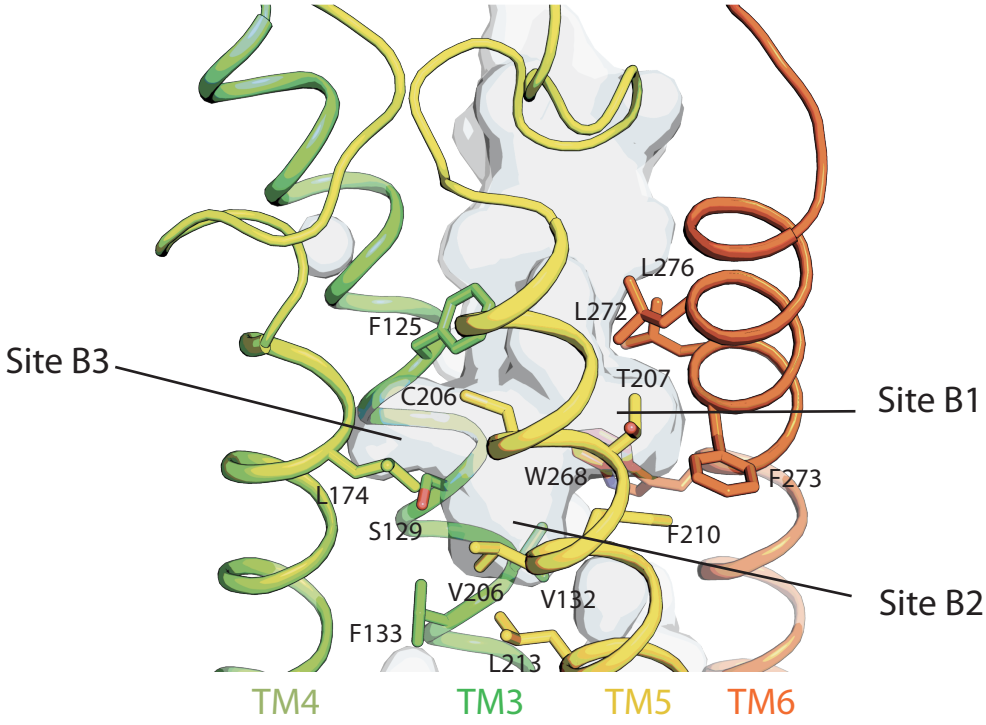

Supplementary Figure 6. Residues in the side binding pockets B1, B2 and B3 in $S1P_1$. The cartoon structure of $S1P_1$ is overalyed with the slice through view of the ligand binding pockets of $S1P_1$ with the side binding pockets B1, B2 and B3 indicated. The sidechains of the residues in B1, B2 and B3 are shown.

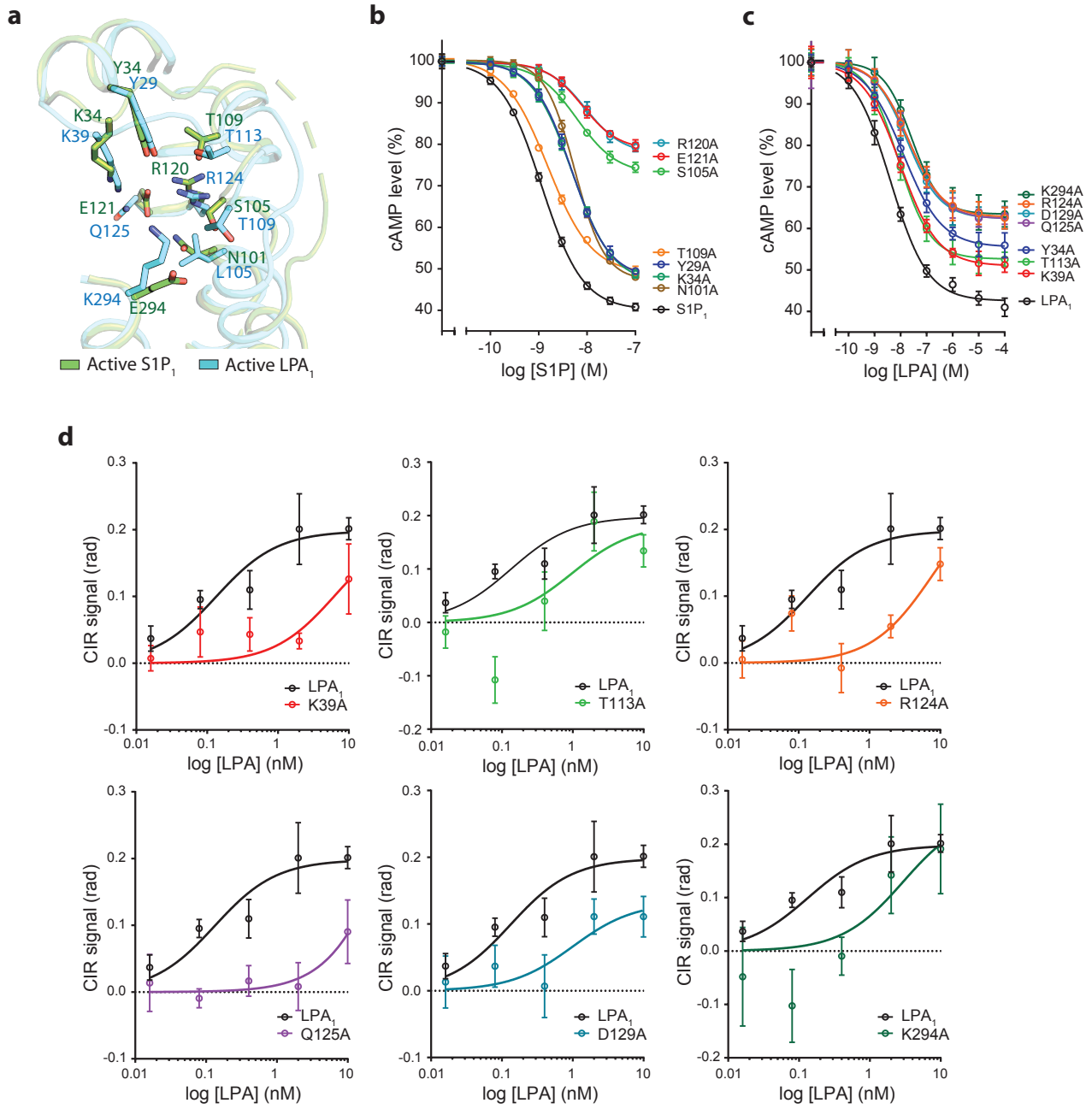

Supplementary Figure 7. **Functional studies of residues in $S1P_1$ and LPA_1**. (**a**) Comparison of the active $S1P_1$ and the active LPA_1 structures with critical residues shown. (**b**) cAMP assays of wild-type and mutant $S1P_1$ in CHO cells. (**c**) cAMP assays of wild-type and mutant LPA_1 in B103 cells. (**d**) Ligand-binding assays of wild-type and mutant LPA_1 in B103 cells. Wild-type (WT, in black color), and various mutants of LPA_1 were stably expressed in B103 cells. A free solution assay, where the receptor (LPA_1/mutants) containing nanovesicles and unlabeled 18:1 LPA ligand were freely moving into solution, was used in a native environment of the binding partners (18:1 LPA-LPA_1) (see the Methods). Individual curves from the mutants were comapred with the same curve from the wild-type receptor. Data are shown as mean ± SD. n = 3 independent experiments. Source data are provided as a Source Data file.

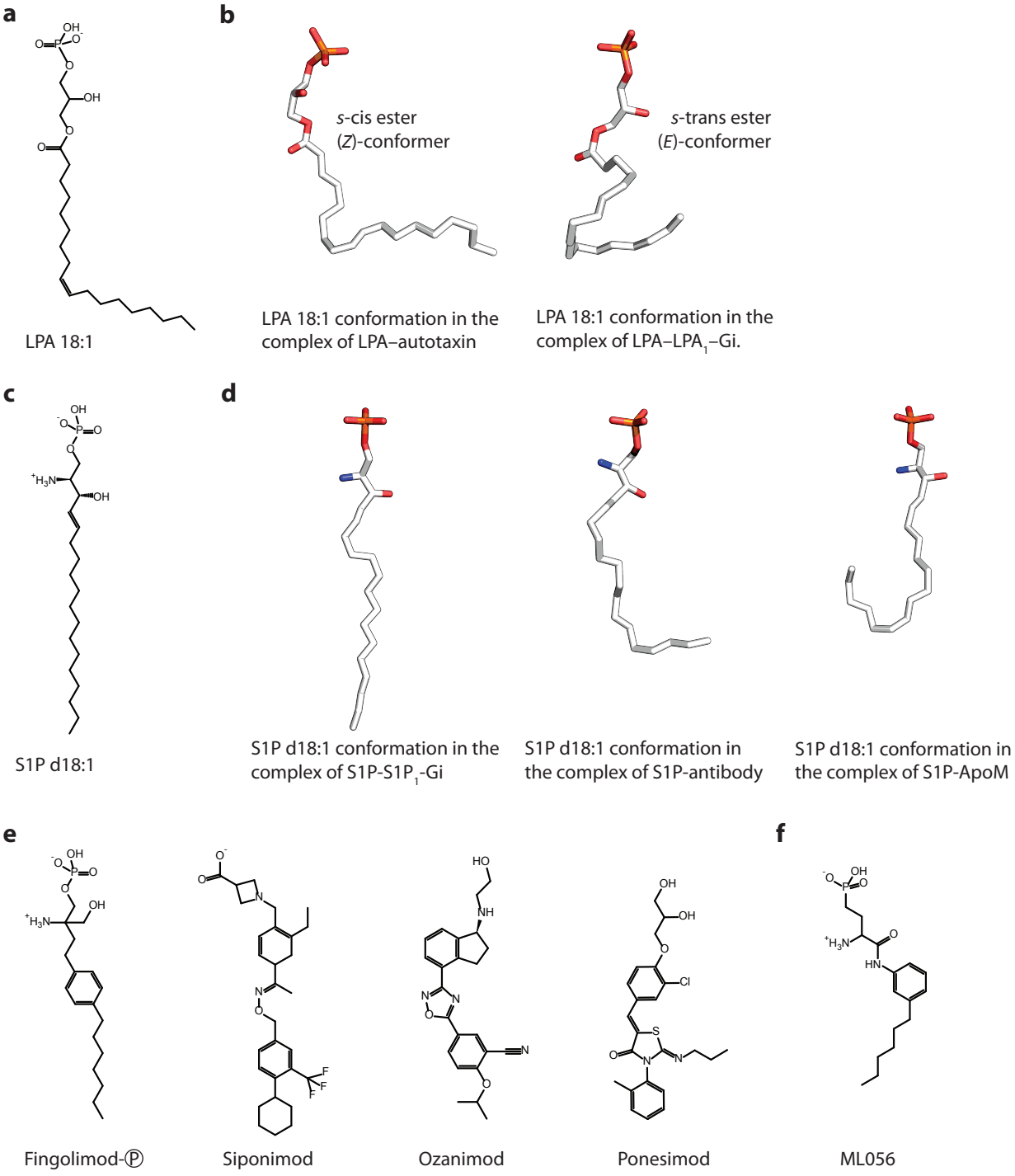

Supplementary Figure 8. Chemical conformations of ligands for LPA and S1P receptors. (***a***) Chemical structure of LPA 18:1. (**b**) Structures of LPA 18:1 in the complex of LPA–autotaxin or of LPA–LPA_1–Gi. (**c**) Chemical structure of S1P d18:1. (**d**). Structures of S1P d18:1 in the complex of S1P–$S1P_1$–Gi, S1P–antibody, or S1P–ApoM. (**e**) Chemical structures of S1P receptor-targeting MS-treatment drugs. (**f**) Chemical structure of the $S1P_1$ antagonist ML056.

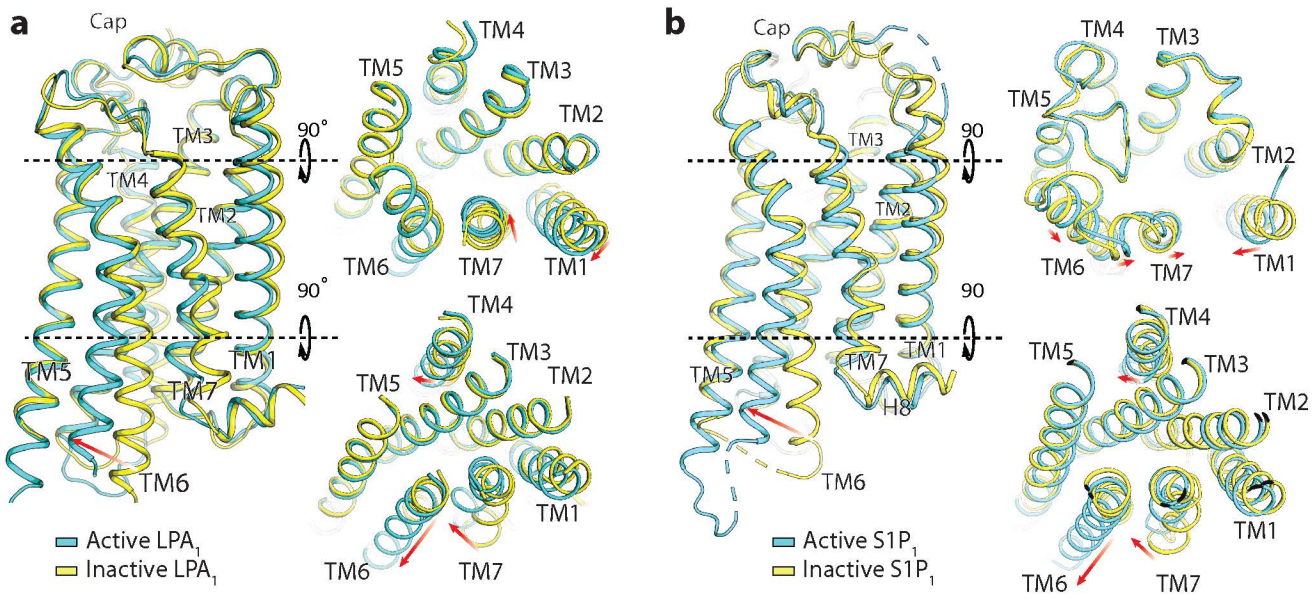

Supplementary Figure 9. Structural comparisons of inactive and active LPA_1 and $S1P_1$. a, Structural comparison of the inactive (PDB 4Z34) and active (current study) states of LPA_1. **b,** Structural comparison of the inactive (PDB 3V2Y) and active (current study) states of $S1P_1$.

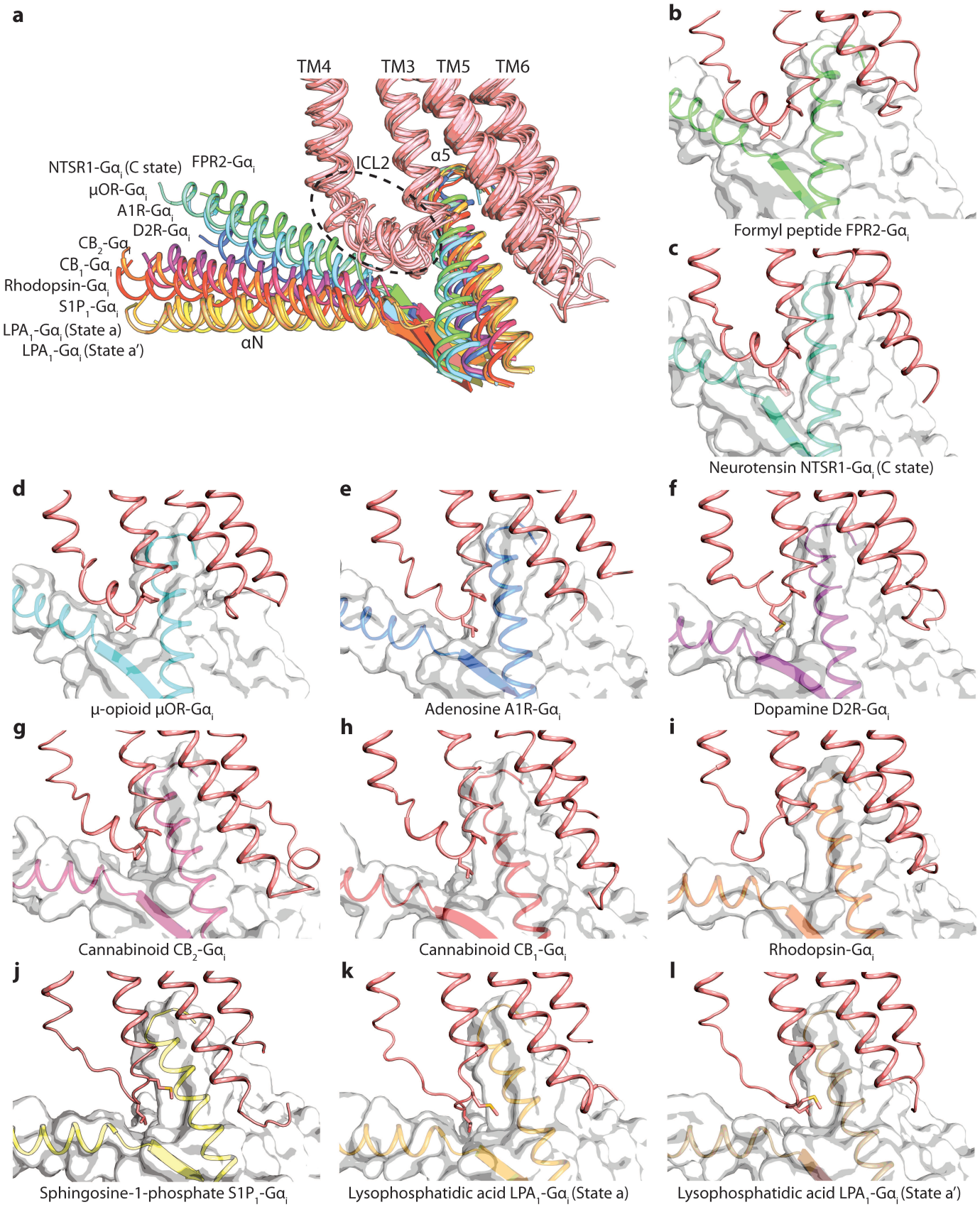

Supplementary Figure 10. Comparisons of the interactions between ICL2 of family A GPCRs and Gα$_i$. An ensemble (**a**) and individual (**b-l**) displays are presented to show Gα$_i$ interactions with ICL2 of FPR2 (PDB: 6omm), Neurotensin (C state) (PDB: 6os9), μOR (PDB: 6dde), A1R (PDB: 6d9h), D2R (PDB: 6vms), CB_2 (PDB: 6pt0), CB_1 (PDB: 6n4b), Rhodopsin (PDB: 6cmo), $S1P_1$ (this work), LPA_1 (State a) (this work) and LPA_1 (State a') (this work).

LPA$_1$ Gα$_i$ β$_1$γ$_2$ w/ Lysophosphatidic Acid
Processing of the cluster analysis-isolated states

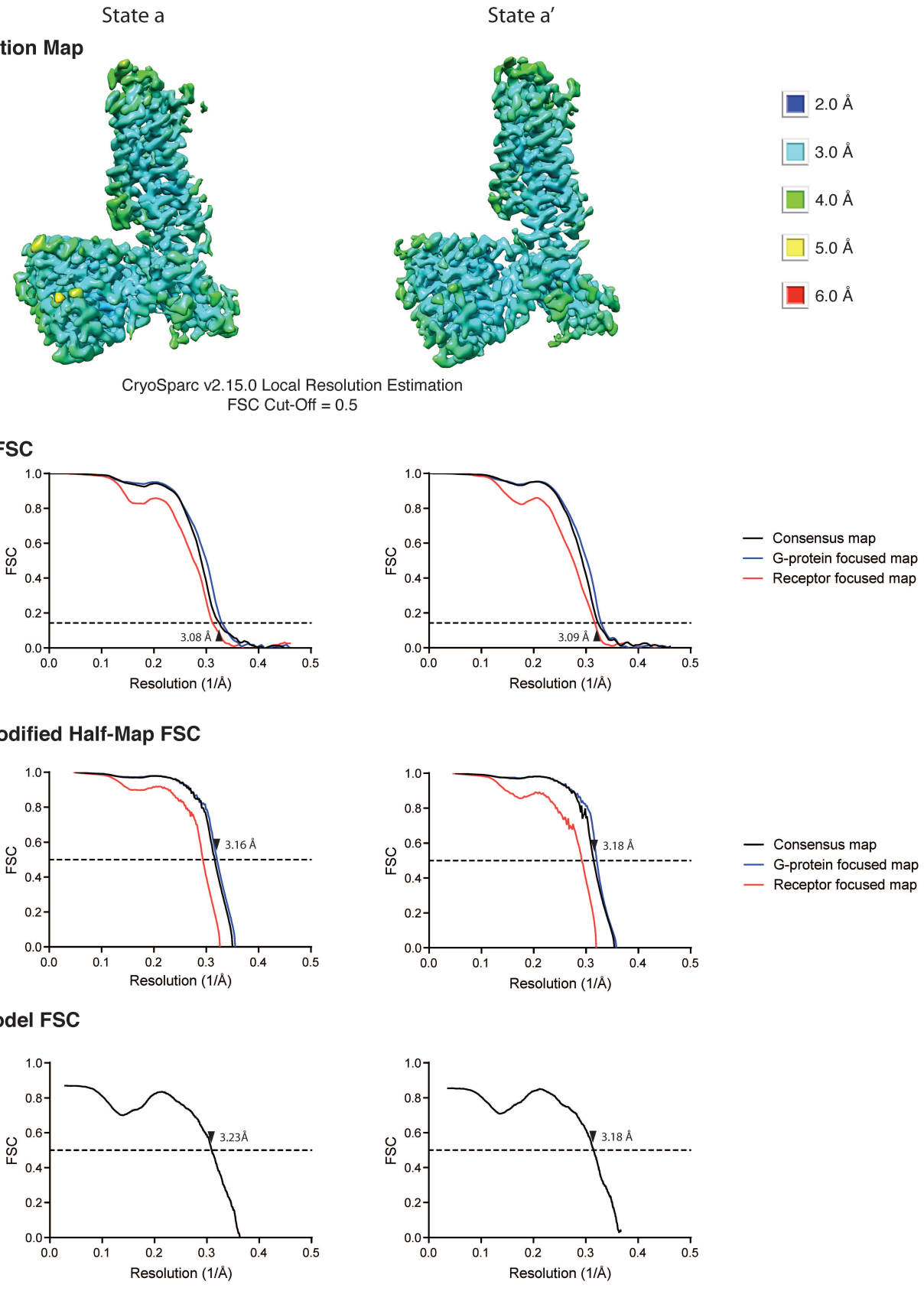

Supplementary Figure 11. 3D variability analysis (3DVA) in CryoSparc v2 was used to cluster particles based on principal components of movement. Manual inspection of the maps generated from 20 clusters led to the identification of two farthest positionings for the G-protein relative to the GPCR. Clusters that fit either position were grouped, and our standard processing workflow was used to generate density modified composite maps for each state (see Materials & Methods for details). (**a**) Local resolution maps for both states. (**b**) Half-map FSC curves for the consensus, G-protein focused, and GPCR focused refinements for both states. (**c**) Half-map FSC curves after applying density modification to each refinement for both states. (**d**) Map-to-model FSC curves for the final models refined against a composite map of the three density-modified refinements.

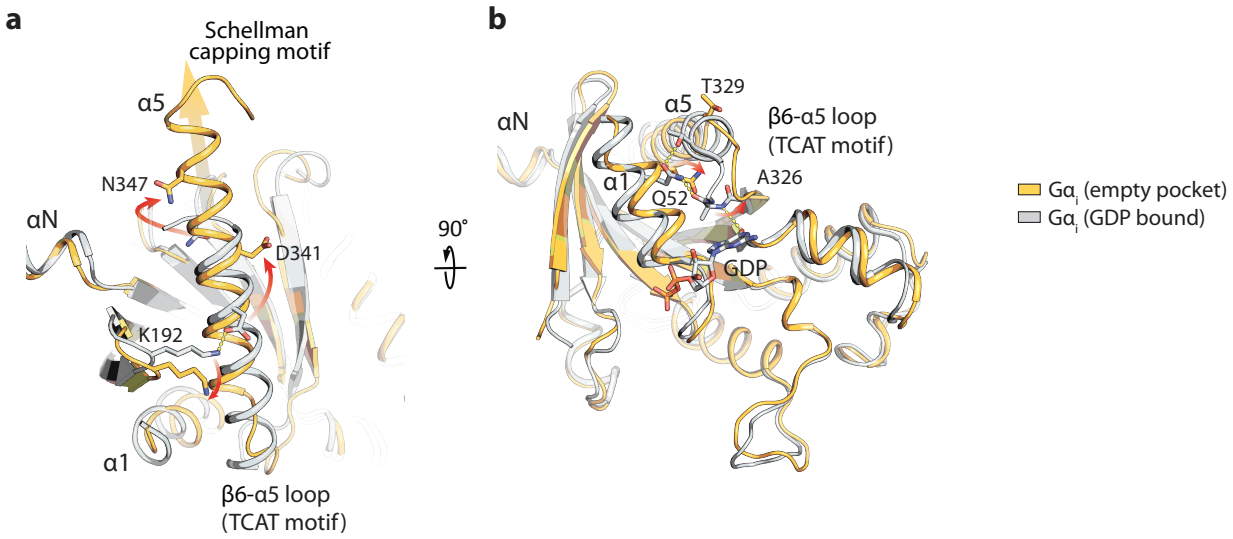

Supplementary Figure 12. Structural basis of the activation of Gi by LPA-bound LPA_1. **(a)** Disruptions of intra-molecular interactions of G**α**$_i$ during Gi activation by LPA-bound LPA_1. An ionic interaction between the sidechain of D341 in the **α**5-helix and the sidechain of K192 in the β2-β3 loop in the inactive G**α**$_i$(GDP)Gβγ trimer (in gray) is broken. D341 forms new interactions with K345 and E318 in the complex of LPA–LPA_1–Gi (in light orange). **(b)** An interacting network involving the sidechain of Q52 in the **α**1-helix, the backbone carbonyl of A326 in the β6-**α**5 loop, and the sidechain of T329 in the **α**5-helix is disrupted.

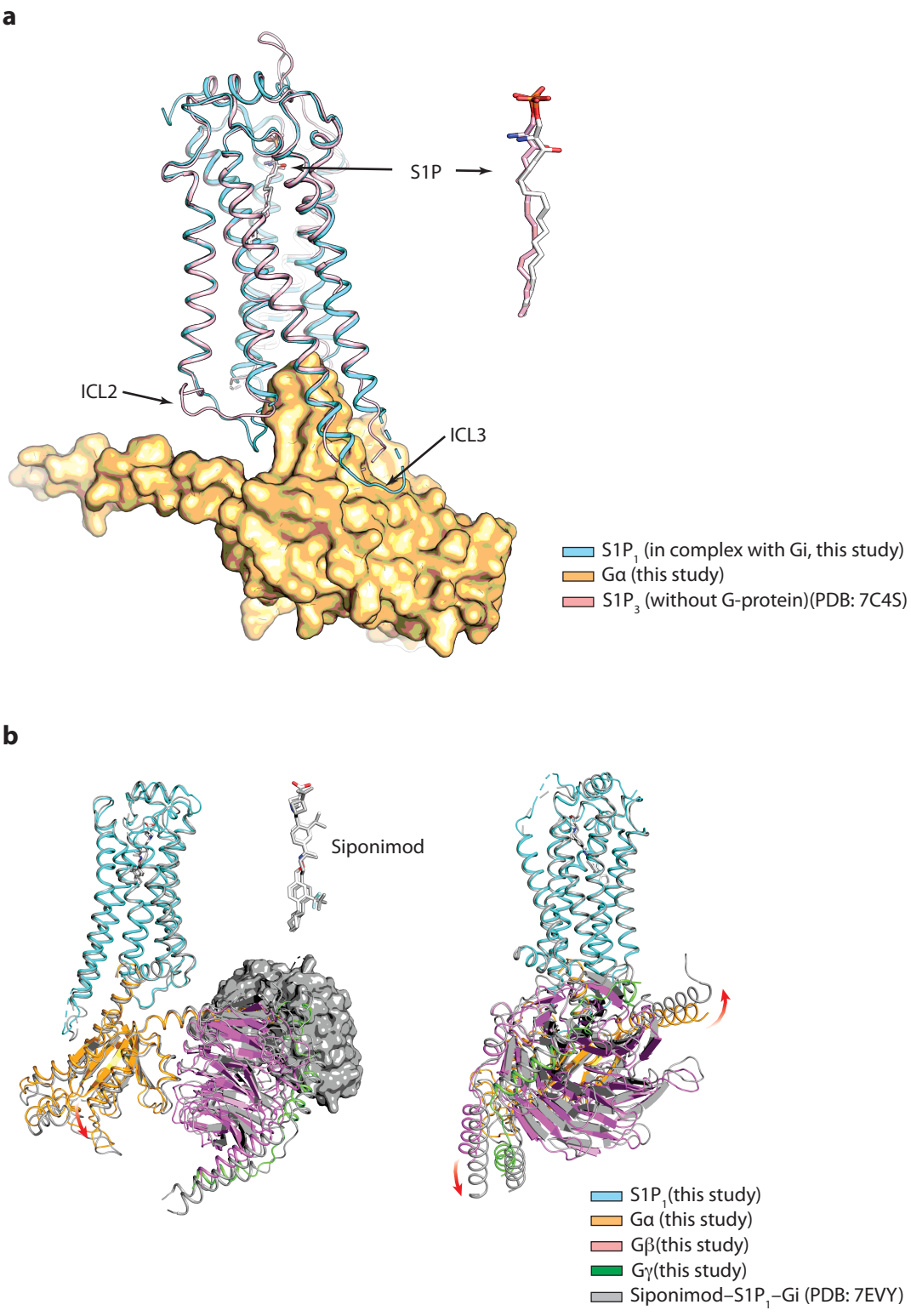

Supplementary Figure 13. Structural comparisons. a, Comparison of the complex of S1P–$S1P_1$-Gi and S1P–$S1P_3$ (without G-protein). $S1P_1$ and $S1P_3$ have similar S1P-binding pockets with similar S1P conformation. **b,** Comparison of the complex of Siponimod–$S1P_1$-Gi from the current study and the one recently published (PDB 7EVY). While the conformations of S1P1 and Siponimod are similar, the positions of Gi-proteins are slightly different.